*38th International Electric Vehicle Symposium and Exhibition (EVS38)*
*Göteborg, Sweden, June 15-18, 2025*

# Development of a Control-Oriented Thermal Management Model for BEVs with Heat Pump-Based HVAC Systems

Prashant Lokur[1], Nikolce Murgovski[1], and Mikael Larsson[2]

[1]*Dept. of Electrical Engineering, Chalmers University of Technology, SE-412 96 Gothenburg, Sweden*
*lokur@chalmers.se, nikolce.murgovski@chalmers.se*
[2]*Dept. of Thermal Energy Management, Zeekr Technology Europe, SE-417 55 Gothenburg, Sweden*

**Executive Summary**

This paper introduces a control-oriented modeling framework for thermal energy management (TEM) in battery electric vehicles (BEVs), specifically designed to support real-time predictive and optimization-based control strategies. Developed from a detailed open source MathWorks reference model, the proposed approach strategically simplifies complex thermal interaction between coolant loops, heat pump-based heating, ventilation and air conditioning (HVAC) dynamics, and cabin air thermal behavior. Key features include simplified thermal dynamics and a modular structure that supports different operating modes, making the model suitable with real-time predictive control strategies such as Model Predictive Control (MPC). Validation against the high-fidelity model demonstrates that the control-oriented model achieves a mean absolute temperature prediction error below 1.45 °C, while reducing simulation time by approximately 85 %. Provided as an open-source solution, the proposed model serves as a robust and accessible tool for collaborative research and development, facilitating the advancement of energy-efficient TEM control strategies to effectively mitigate BEV range anxiety under extreme weather conditions.

*Keywords: Electric Vehicles, Thermal management, Energy Management, Advanced controls of EV and Modeling and Simulation*

## 1 Introduction

Battery Electric Vehicles (BEVs) are central to the global shift toward sustainable transportation, driven by stricter emission regulations, and the growing adoption of renewable energy sources [1]. However, despite their environmental and efficiency advantages, BEVs still face significant challenges  most notably range anxiety, i.e., limited driving range under real-world conditions, which continues to hinder widespread adoption [2–4].

Studies have shown that extreme weather conditions can reduce BEV range by 30 % to 35 % [5]. In controlled testing at Argonne National Laboratory, a Ford Focus EV experienced range reductions of 53.7 % in hot weather and 59.3 % in cold weather during Urban Dynamometer Driving Schedule (UDDS) cycles [6]. These reductions are primarily due to increased energy consumption by the Thermal Energy Management (TEM) system, which draws significant power to ensure passenger comfort and maintain safe operating temperatures for components such as battery, motor, and power electronics [5, 6]. While larger battery packs can help mitigate range limitations, they introduce penalties in terms of cost and vehicle weight, potentially undermining the efficiency and appeal of BEVs. Therefore, improving overall energy efficiency particularly through optimized thermal management offers a more practical and cost-effective approach to extending driving range and enhancing user satisfaction.
Advanced TEM systems with heat pump-based heating, ventilation and air conditioning (HVAC) and reconfigurable coolant loops are key to improving BEV energy efficiency [7, 8]. These systems enable dynamic reconfiguration and waste heat recovery, offering significant energy savings [9]. However, current studies typically focus on isolated subsystems such as HVAC [10–15] or Battery Thermal Energy Management System [16–19], lacking integration of refrigerant, coolant, and cabin dynamics. This limits the development of holistic control strategies that are both accurate and computationally efficient. Although system-level models increase control complexity, this can be mitigated by developing Control-Oriented Models (COMs) that balance fidelity with real-time feasibility. While some integrated models exist [20], their proprietary nature restricts broader research use.
High-fidelity simulation tools, such as those provided by MathWorks [21], are indispensable for detailed system design and understanding nonlinear dynamics. However, their computational intensity and nonsmooth behavior make them unsuitable for real-time embedded controllers. This creates a critical gap: advanced control methodologies like Model Predictive Control (MPC) effective for optimal control in automotive applications [22, 23] require models that balance accuracy with computational tractability. Additionally, the scarcity of publicly available, open-source TEM models hinders collaborative research, as existing high-fidelity models are typically proprietary [21]. This lack of open benchmarks complicates efforts to validate novel control strategies or explore comprehensive integrated TEM solutions.
To address these gaps, this paper introduces a systematic methodology for developing a COM tailored for BEV TEM systems equipped with reconfigurable parallel-serial coolant loops and heat pump-based HVAC systems. Derived from a high-fidelity reference model, the proposed COM simplifies noncritical dynamics while preserving thermal behaviors of the system, enabling real-time control applications. Key advancements include:

- Integration of coolant loops, refrigerant transitions (heat pump/cold modes), and cabin air dynamics into a unified framework;
- Physics-based simplifications (e.g., lumped thermal masses, precomputed refrigerant properties) that retain system-level fidelity while reducing computational time;
- An open-source implementation that promotes accessibility, enabling researchers to validate control strategies (e.g., MPC) and accelerate innovation in energy-optimal TEM.

The remainder of the paper is organized as follows: Section 2 describes the BEV TEM architecture and reference model. Section 3 details the COM development methodology. Section 4 outlines the parameter tuning. Section 5 presents results evaluating model accuracy and computational efficiency. Finally, Section 6 concludes with future research directions.

# 2 System Architecture

The TEM system of the BEVs under consideration, shown in Fig. 1, integrates multiple fluid loops (coolant, refrigerant, and cabin air) configured to handle varying operating conditions. By switching between serial and parallel modes for the coolant loops, as well as transitioning the refrigerant loop between cold loop and heat pump modes, the system ensures the battery and powertrain components are within desired temperature limits while also delivering thermal comfort to the vehicles occupants.
The two liquid coolant loops can be configured either in series or parallel mode via directional valves. At low ambient temperatures, the loops are arranged in series to allow waste heat from the electric motor, inverter, DCDC converter to warm the battery pack. If necessary, an auxiliary heater supplements the thermal energy. Under moderate ambient conditions, the radiator cools both the batteries and power electronics efficiently. When ambient temperatures exceed 35 °C, the system switches to parallel loop operation. In this configuration, one loop cools

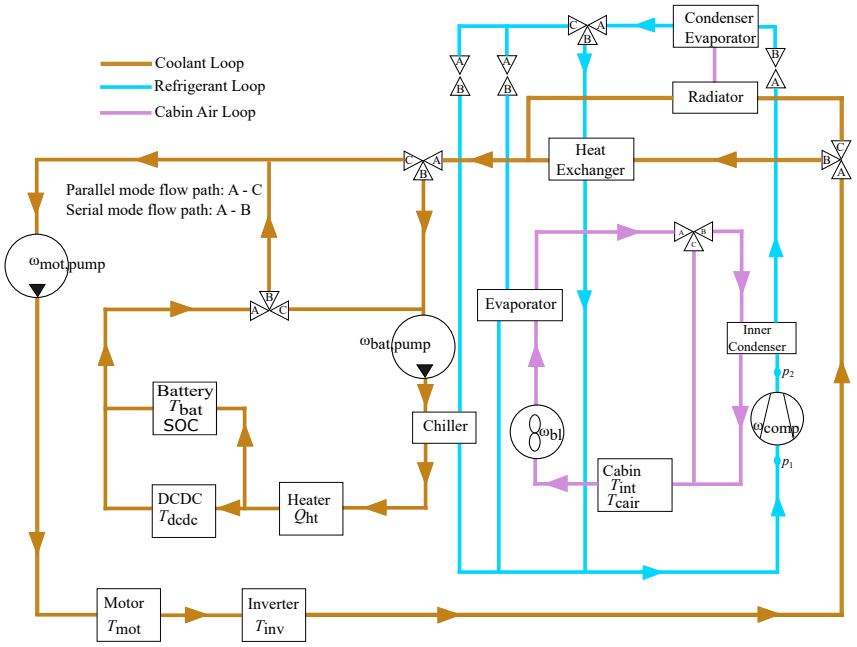


**Fig. 1.** Schematic of the BEVs Thermal Energy Management (TEM) system, showing dual-mode coolant loops, the refrigerant loop, and cabin HVAC integration.

the powertrain via the radiator, while the second loop utilizes a chiller connected to the refrigerant loop to cool the battery pack independently.

The refrigerant loop operates in two distinct modes: cold loop mode and heat pump mode. In cold loop mode, the cabin air bypasses the inner condenser, and the heat pump expansion valve remains fully open. The condenser/evaporator rejects heat to the environment, while the chiller expansion valve cools the coolant, and the evaporator expansion valve cools the cabin air. In cold ambient conditions, the system transitions to heat pump mode, wherein the inner condenser is used to heat the cabin air. In this mode, the condenser/evaporator acts as an evaporator to absorb heat from the ambient environment. The heat pump expansion valve meters the refrigerant, and a bypass around the evaporator and chiller directs refrigerant to a heat exchanger that extracts additional waste heat from the powertrain coolant circuit, thereby improving overall system efficiency.

# 3 Dynamic Modeling of the BEV Thermal Management System

A COM for the BEV thermal management system is developed under cold climate conditions, with the ambient temperature set to $-10\,^{\circ}\mathrm{C}$. The simulation assumes a cold-start scenario, where all thermal components begin at ambient temperature. The model state vector captures compressor inlet pressure $p_1$, compressor outlet pressure $p_2$, battery state of charge SOC, battery temperature $T_\mathrm{b}$, inverter temperature $T_\mathrm{inv}$, motor temperature $T_\mathrm{mot}$, DC/DC converter temperature $T_\mathrm{dcdc}$, cabin air temperature $T_\mathrm{cair}$, and cabin interior temperature $T_\mathrm{int}$. The state vector $x$ is defined as

$$x(t) = \begin{bmatrix} \mathrm{SOC}(t) & p_1(t) & p_2(t) & T_\mathrm{b}(t) & T_\mathrm{inv}(t) & T_\mathrm{mot}(t) & T_\mathrm{dcdc}(t) & T_\mathrm{cair}(t) & T_\mathrm{int}(t) \end{bmatrix}^\top. \tag{1}$$

The control input vector consists of actuator commands for the battery coolant pump speed $\omega_\mathrm{bat,pump}$, motor coolant pump speed $\omega_\mathrm{mot,pump}$, compressor speed $\omega_\mathrm{comp}$, HVAC blower speed $\omega_\mathrm{bl}$, and thermal power input $Q_\mathrm{ht}$. The control vector $u$ is defined as

$$u(t) = \begin{bmatrix} \omega_\mathrm{bat,pump}(t) & \omega_\mathrm{mot,pump}(t) & \omega_\mathrm{comp}(t) & \omega_\mathrm{bl}(t) & Q_\mathrm{ht}(t) \end{bmatrix}^\top. \tag{2}$$

## 3.1 Traction Power and Component Losses

The open-source high-fidelity MathWorks reference model estimates component losses (e.g., motor, inverter, battery) via lookup tables mapped to vehicle speed. While this enables rapid simulation, it limits adaptability to

**Table 1.** Vehicle Specifications Used in the Simulation

| Parameter | Symbol | Value |
|---|---|---|
| Vehicle Mass | $m$ | 1200 kg |
| Wheel Radius | $r_{\text{wheel}}$ | 0.3 m |
| Frontal Area | $A_{\text{f}}$ | 2 $\text{m}^2$ |
| Drag Coefficient | $C_{\text{d}}$ | 0.30 |
| Rolling Resistance Coefficient | $C_{\text{rr}}$ | 0.015 |
| Gear Ratio | $N_{\text{gr}}$ | 8 |
| Gear Efficiency | $\eta_{\text{gear}}$ | 0.98 |
| Air Density | $\rho_{\text{air}}$ | 1.225 $\text{kg m}^{-3}$ |
| Gravitational Acceleration | $g$ | 9.81 $\text{m s}^{-2}$ |
| Low Side Voltage | $V_{\text{dc}}$ | 12 V |

diverse vehicle platforms. To enhance generalization, authors have recalibrated traction power demand using first-principles vehicle dynamics based on vehicle parameters summarized in Table 1. The total tractive force $F_{\text{traction}}$ is derived from mechanical equilibrium [24] as

$$\begin{aligned} F_{\text{traction}}(t) &= F_{\text{rolling}}(t) + F_{\text{aero}}(t) + F_{\text{gravity}}(t) + F_{\text{inertia}}(t) \\ &= C_{\text{rr}} mg\cos(\theta(t)) + \frac{1}{2}\rho_{\text{air}} C_{\text{d}} A_{\text{f}} v(t)^2 + mg\sin(\theta(t)) + ma(t), \end{aligned} \tag{3}$$

where $v$ is vehicle speed, $a$ is longitudinal acceleration, $m$ is the vehicle mass, $g$ is gravitational acceleration, $\rho_{\text{air}}$ is the air density, $\theta$ is the road grade angle, and $C_{\text{rr}}$, $C_{\text{d}}$, $A_{\text{f}}$ denote the rolling resistance coefficient, aerodynamic drag coefficient, and frontal area, respectively.
The electrical power demand at the motor is expressed as

$$P_{\text{motor,elec}}(t) = \frac{F_{\text{traction}}(t)v(t)}{\eta_{\text{gear}}^{\text{sign}(F_{\text{traction}}(t))}} + P_{\text{motor,loss}}(\tau_{\text{motor}}(t), \omega_{\text{motor}}(t)) \tag{4}$$

where $\eta_{\text{gear}}$ is the gear efficiency, $\omega_{\text{motor}}$ is the motor angular velocity, and $\tau_{\text{motor}}$ is the motor torque demand. The motor loss $P_{\text{motor,loss}}$ is interpolated from experimental loss maps as a function of motor torque and speed.
The total electrical power demand from the battery is expressed as

$$P_{\text{b}}(t) = P_{\text{motor,elec}}(t) + P_{\text{inverter,loss}}(\tau_{\text{motor}}(t), \omega_{\text{motor}}(t)) + P_{\text{loss,dc}}(t) + P_{\text{TEM}}(t) \tag{5}$$

$$P_{\text{TEM}}(t) = P_{\text{comp}}(t) + P_{\text{bat,pump}}(t) + P_{\text{mot,pump}}(t) + P_{\text{blower}}(t) + P_{\text{rad,fan}}(t) \tag{6}$$

Here, $P_{\text{inverter,loss}}$ represents inverter losses (from lookup tables based on motor torque and speed), $P_{\text{loss,dc}}$ is the power loss in the DC-DC converter, and $P_{\text{TEM}}$ is the aggregate power consumption of thermal energy management components, including the compressor, pumps, blower, and radiator fan.
The DC-DC converter losses are calculated by accounting for conduction and switching losses in both Insulated-Gate Bipolar Transistor (IGBT) and diode devices [25–27] and is expressed as

$$\begin{aligned} P_{\text{loss,dc}}(t) = {} & \left(V_{\text{ce0}} I_{\text{l}}(t) + r_{\text{ce}} I_{\text{l}}^2(t)\right) D + \left(V_{\text{d0}} I_{\text{l}}(t) + r_{\text{d}} I_{\text{l}}^2(t)\right)(1-D) + E_{\text{sw}} f_{\text{sw}} \left(\frac{I_{\text{l}}(t)}{I_{\text{ref}}}\right)^{K_{\text{it}}} \left(\frac{V_{\text{dc}}}{U_{\text{ref}}}\right)^{K_{\text{vt}}} \\ & + E_{\text{rec}} f_{\text{sw}} \left(\frac{I_{\text{l}}(t)}{I_{\text{ref}}}\right)^{K_{\text{id}}} \left(\frac{V_{\text{dc}}}{U_{\text{ref}}}\right)^{K_{\text{vd}}} \end{aligned} \tag{7}$$

where, $V_{\text{ce0}}$ and $r_{\text{ce}}$ denote the IGBT's forward voltage drop and on-state resistance, while $V_{\text{d0}}$ and $r_{\text{d}}$ represent the diode's forward voltage drop and on-state resistance. $D$ is the converter duty ratio, $I_{\text{l}}$ is the low voltage side current drawn from the battery, and $V_{\text{dc}}$ is the DC-link voltage. The switching frequency is denoted by $f_{\text{sw}}$, and $E_{\text{sw}}$ is the total energy lost per switching event in the IGBT (including both turn-on and turn-off losses), while $E_{\text{rec}}$ is the reverse recovery energy loss in the diode. The parameters $I_{\text{ref}}$ and $U_{\text{ref}}$ are normalization constants (reference current and voltage) used to linearize the switching loss behavior. The empirical coefficients $K_{\text{it}}$, $K_{\text{vt}}$, $K_{\text{id}}$, and $K_{\text{vd}}$ scale the influence of current and voltage on the switching losses for the IGBT and diode, respectively. The low-voltage side current $I_{\text{l}}(t)$ is estimated by dividing the low-voltage side power demand $\left(P_{\text{TEM}}(t) - P_{\text{comp}}(t)\right)$ by the

low-voltage bus voltage.

## 3.2 Battery Electrical-Thermal Model

The battery is modeled as a voltage source $O_{\mathrm{ocv}}$ connected in series with an internal resistance $R_{\mathrm{b}}$. The battery current $I_{\mathrm{b}}$ is expressed as

$$I_{\mathrm{b}}(t) = \frac{1}{2R_{\mathrm{b}}(\mathrm{SOC}(t), T_{\mathrm{b}}(t))} \left( O_{\mathrm{ocv}}(\mathrm{SOC}(t), T_{\mathrm{b}}(t)) - \sqrt{O_{\mathrm{ocv}}^2(\mathrm{SOC}(t), T_{\mathrm{b}}(t)) - 4P_{\mathrm{b}}(t)R_{\mathrm{b}}(\mathrm{SOC}(t), T_{\mathrm{b}}(t))} \right) \tag{8}$$

where SOC is the battery state of charge and $T_{\mathrm{b}}$ is the battery temperature.
The open-circuit voltage $O_{\mathrm{ocv}}$ is modeled as a second-order polynomial in both SOC and temperature

$$O_{\mathrm{ocv}}(\mathrm{SOC}(t), T_{\mathrm{b}}(t)) = \sum_{i=0}^{2}\sum_{j=0}^{2} \mu_{ij}\,\mathrm{SOC}^i(t)\,T_{\mathrm{b}}^j(t), \;\; R_{\mathrm{b}}(\mathrm{SOC}(t), T_{\mathrm{b}}(t)) = \sum_{i=0}^{2}\sum_{j=0}^{2} \psi_{ij}\,\mathrm{SOC}^i(t)\,T_{\mathrm{b}}^j(t) \tag{9}$$

where $\mu_{ij}$ and $\psi_{ij}$are polynomial coefficients identified from the MathWorks model data specifications.The state of charge of the battery is expressed as

$$\frac{\mathrm{d}\,\mathrm{SOC}(t)}{\mathrm{dt}} = -\frac{I_{\mathrm{b}}(t)}{Q_{\mathrm{nom}}} \tag{10}$$

where $Q_{\mathrm{nom}}$ is the nominal battery capacity.
BEVs generate significant heat during operation due to electrical losses (e.g., Joule heating, switching losses) in components such as the inverter, DC/DC converter, and motor, as well as mechanical friction in the drivetrain. Accurate thermal modeling requires precise estimation of these heat generation rates, which are directly approximated from their respective power losses in this work. This approach leverages the first-law equivalence between electrical/mechanical power losses and thermal energy dissipation. Specifically, the heat generation rates for the inverter $Q_{\mathrm{inv}}$, motor $Q_{\mathrm{motor}}$, and DC/DC converter $Q_{\mathrm{dcdc}}$ are expressed as

$$Q_{\mathrm{inv}}(t) = P_{\mathrm{inverter,loss}}(\tau_{\mathrm{motor}}(t), \omega_{\mathrm{motor}}(t)), \;\; Q_{\mathrm{motor}}(t) = P_{\mathrm{motor,loss}}(\tau_{\mathrm{motor}}(t), \omega_{\mathrm{motor}}(t)), \;\; Q_{\mathrm{dcdc}}(t) = P_{\mathrm{dcdc,loss}}(t). \tag{11}$$

The battery's heat generation rate $Q_{\mathrm{gen}}$ is estimated using a lumped thermal mass model [16] and is expressed as

$$Q_{\mathrm{gen}}(t) = I_{\mathrm{b}}^2(t)R_{\mathrm{b}}(\mathrm{SOC}(t), T_{\mathrm{b}}(t)) - I_{\mathrm{b}}(t)T_{\mathrm{b}}(t)\Theta + I_{\mathrm{b}}^2(t)R_{\mathrm{br}} \tag{12}$$

where $\Theta$ is the entropic heating coefficient and $R_{\mathrm{br}}$ is the bus bar resistance used to connect different cell modules within the battery pack.

## 3.3 Coolant Loop Simplifications

In cold climates, coolant loops operate in series mode to prioritize waste heat recovery. The coolant mass flow rate at the battery coolant pump and motor coolant pump $\dot{m}_{\mathrm{c,clnt}}$ $c \in \{\mathrm{battery}, \mathrm{motor}\}$ is expressed as

$$\dot{m}_{\mathrm{c,clnt}}(t) = \omega_{\mathrm{c,pump}}(t) \cdot V_{\mathrm{disp,c}} \cdot \rho_{\mathrm{clnt}} \cdot \eta_{\mathrm{c,pump}} \tag{13}$$

where $\omega_{\mathrm{c,pump}}$ is the pump speed, $V_{\mathrm{disp,c}}$ is the pump displacement, $\rho_{\mathrm{clnt}}$ is the coolant density, and $\eta_{\mathrm{c,pump}}$ is the pump volumetric efficiency.
The coolant pump power consumption $P_{\mathrm{c,pump}}$ is expressed as

$$P_{\mathrm{c,pump}}(t) = \frac{\dot{m}_{\mathrm{c,clnt}}(t)\Delta p(t)/\rho_{\mathrm{clnt}}}{\eta_{\mathrm{pump,elec}}} \tag{14}$$

where $\Delta p$ is the total pressure drop across the cooling circuit and $\eta_{\mathrm{c,pump}}$ is the electrical efficiency of the pump. The pressure drop $\Delta p$ is estimated as the summation of the pressure drops across all individual components (e.g., motor, inverter) within the coolant loop. Another simplification adopted in the coolant loop is the modeling of the heater. The heater is modeled by assuming that the input electrical power is converted into thermal power added

to the coolant, scaled by a heating efficiency $\eta_{\mathrm{ht}}$. The outlet temperature of the coolant after the heater is then expressed as

$$T_{\mathrm{clnt,ht,out}}(t) = T_{\mathrm{clnt,ht,in}}(t) + \frac{\eta_{\mathrm{ht}} Q_{\mathrm{ht}}(t)}{\dot{m}_{\mathrm{bat,clnt}}(t) c_{p,\mathrm{clnt}}} \tag{15}$$

where $c_{p,\mathrm{clnt}}$ is the specific heat capacity of the coolant.

## 3.4 Component Thermal Models

The heat generated by battery, inverter, DC/DC converter, and motor during the operation is thermally managed via liquid coolant loops. These components are modeled as lumped thermal masses [20]. This approach simplifies distributed thermal gradients into single-node representations. The thermal dynamics of each component $i \in \{\mathrm{battery}, \mathrm{inverter}, \mathrm{dcdc}, \mathrm{motor}\}$ are expressed as

$$m_i c_{p,i} \frac{\mathrm{d}T_i(t)}{\mathrm{d}t} = \alpha_i \left( \dot{Q}_{\mathrm{gen},i}(t) - \dot{Q}_{\mathrm{cool},i}(t) \right) \tag{16}$$

where $m_i$ is the thermal mass, $c_{p,i}$ is the specific heat, $\dot{Q}_{\mathrm{gen},i}$ is the heat generation given by (11)–(12), $\alpha_i$ is a tuning coefficient and $\dot{Q}_{\mathrm{cool},i}$ is the heat extracted by the coolant. The heat transfer from component $i$ to the coolant, $\dot{Q}_{\mathrm{cool},i}$, consists of convection $\dot{Q}_{\mathrm{conv},i}$ and conduction $\dot{Q}_{\mathrm{cond},i}$ contributions and is estimated as

$$\dot{Q}_{\mathrm{conv},i}(t) = \dot{m}_{\mathrm{c,clnt}}(t) c_{p,\mathrm{clnt}} \left( T_i(t) - T_{\mathrm{clnt,in},i}(t) \right) \left( 1 - e^{-\frac{\beta_i K_{\mathrm{conv},i}}{\dot{m}_{\mathrm{clnt},i}(t) c_{p,\mathrm{clnt}}}} \right) \tag{17}$$

$$\dot{Q}_{\mathrm{cond},i}(t) = \vartheta_i K_{\mathrm{c},i} \left( T_i(t) - T_{\mathrm{clnt,in},i}(t) \right) \tag{18}$$

where $\dot{m}_{\mathrm{c,clnt}}$ is the coolant mass flow rate through component $i$, $T_i(t)$ is the component temperature, and $T_{\mathrm{clnt,in},i}(t)$ is the inlet coolant temperature. $K_{\mathrm{conv},i}$ and $K_{\mathrm{cond},i}$ are the effective convective and conductive heat transfer coefficients, respectively. The coolant inlet temperature $T_{\mathrm{clnt,in},i}$ for each component is assumed to be the coolant outlet temperature from the preceding upstream component in the coolant loop. For example, the battery coolant inlet temperature is assumed to match the heater coolant outlet temperature.

## 3.5 Refrigerant Loop

The refrigerant mass flow rate and compressor power consumption are described through a quasi-static model [28–30]. The refrigerant mass flow rate $\dot{m}_{\mathrm{ref}}$ is expressed as

$$\dot{m}_{\mathrm{ref}}(t) = \eta_{\mathrm{vf}}(t) \omega_{\mathrm{comp}}(t) V_{\mathrm{disp,comp}} \rho_{\mathrm{ref}}, \;\; \eta_{\mathrm{vf}}(t) = \sum_{i=0}^{2} \sum_{j=0}^{2} \kappa_{ij} \left( \frac{p_2(t)}{p_1(t)} \right)^i \omega_{\mathrm{comp}}(t)^j \tag{19}$$

where $\eta_{\mathrm{vf}}$ is the volumetric efficiency, $\omega_{\mathrm{comp}}$ is the compressor speed, $V_{\mathrm{disp,comp}}$ is the compressor displacement volume, $\rho_{\mathrm{ref}}$ is the refrigerant density at the compressor inlet, and $\kappa_{ij}$ are the polynomial fitting coefficients.
The compressor outlet enthalpy $h_2$ is estimated using the inlet enthalpy $h_1$, isentropic outlet enthalpy $h_{2s}$, and isentropic efficiency $\eta_{\mathrm{isen}}$ as

$$h_2(t) = h_1(t) + \frac{h_{2s}(t) - h_1(t)}{\eta_{\mathrm{isen}}}. \tag{20}$$

The isentropic outlet enthalpy $h_{2s}$ is obtained by assuming an isentropic compression from the inlet pressure $p_1$ to the outlet pressure $p_2$, using refrigerant properties computed via CoolProp. The inlet enthalpy $h_1$ is evaluated based on the compressor inlet pressure $p_1$ and the superheat condition of the refrigerant at the compressor inlet.
The power consumption of the compressor $P_{\mathrm{comp}}$ is expressed as

$$P_{\mathrm{comp}}(t) = \frac{\dot{m}_{\mathrm{ref}}(t) \left( h_2(t) - h_1(t) \right)}{\eta_{\mathrm{comp}}} \tag{21}$$

where $\eta_{\mathrm{comp}}$ is the overall efficiency of the compressor.

To capture dynamic refrigerant behavior, the compressor inlet and outlet pressures are estimated from the evaporator and inner condenser dynamics [30], estimated using

$$\sigma_e V_e \left[ (1-\bar{\gamma}_e)\frac{\partial(\rho_l h_l)}{\partial p_1} + \bar{\gamma}_e \frac{\partial(\rho_g h_g)}{\partial p_1} + (\rho_g h_g - \rho_l h_l)\frac{\partial \bar{\gamma}_e}{\partial p_1} + \frac{M_{we} C_e}{V_e}\frac{\partial T_e}{\partial p_1} \right] \frac{dp_1}{dt} = \dot{Q}_e(t) + \dot{m}_{ref}(t)\,(h_4(t) - h_1(t)) \tag{22}$$

$$\sigma_{ic} V_{ic} \left[ (1-\bar{\gamma}_{ic})\frac{\partial(\rho_l h_l)}{\partial p_2} + \bar{\gamma}_{ic} \frac{\partial(\rho_g h_g)}{\partial p_2} + (\rho_g h_g - \rho_l h_l)\frac{\partial \bar{\gamma}_{ic}}{\partial p_2} + \frac{M_{wc} C_{ic}}{V_{ic}}\frac{\partial T_{ic}}{\partial p_2} \right] \frac{dp_2}{dt} = -\dot{Q}_{ic}(t) + \dot{m}_{ref}(t)\,(h_2(t) - h_3(t)) \tag{23}$$

Here, $V_e$ and $V_{ic}$ are the internal volumes of the evaporator and inner condenser, respectively; $\bar{\gamma}_e$ and $\bar{\gamma}_{ic}$ are the mean void fractions; $\rho_l$ and $\rho_g$ are the liquid and vapor densities; and $h_l$, $h_g$ are the respective specific enthalpies. $M_{we}$, $M_{wc}$ represent the thermal mass of the evaporator and condenser walls, while $C_e$, $C_{ic}$ are their specific heat capacities. The wall temperatures $T_e$ and $T_{ic}$ are approximated by the refrigerant saturation temperatures.
The heat transfer rates between refrigerant and air in the evaporator and inner condenser are denoted by $\dot{Q}_e$ and $\dot{Q}_{ic}$, respectively. The refrigerant enthalpy $h_3$ is calculated from the outlet pressure $p_2$ and the refrigerant outlet temperature at the inner condenser. Due to isenthalpic expansion at the valve, $h_4 = h_3$ is assumed. The bracketed terms$[\cdot]$ in (22) and (23) can be precomputed using analytical expressions or lookup tables derived from refrigerant thermodynamic properties.
To model thermal interactions within the refrigerant circuit, heat exchangers are described using the effectiveness - NTU (Number of Transfer Units) method [31]. The heat transfer rate at the inner condenser is estimated using

$$\dot{Q}(t) = \varepsilon(t) C_{min}(t)\,(T_{ref,in}(t) - T_{air,in}(t)) \tag{24}$$

$$\varepsilon(t) = 1 - \exp(-NTU(t)) \tag{25}$$

$$NTU(t) = \frac{U(t)A}{C_{min}(t)}, \quad C_{min}(t) = \min\left(\dot{m}_{ref}(t)c_{p,ref}, \dot{m}_{air}(t)c_{p,air}\right) \tag{26}$$

where, $U(t) = 1/R_{th}(t)$ is the overall heat transfer coefficient, and $A$ is the effective heat transfer area. A special case is considered for phase change processes in the condenser and evaporator, where the refrigerant-side capacity rate becomes large ($\dot{m}_{ref}c_{p,ref} \to \infty$), making $C_{min} = \dot{m}_{air}c_{p,air}$ and allowing effectiveness to be calculated using (25). The total thermal resistance is estimated using

$$R_{th}(t) = \frac{1}{h_{ref}(t)A_{ref}} + R_{wall} + \frac{1}{h_{air}(t)A_{air}} \tag{27}$$

where $h_{ref}$ and $h_{air}$ are the convective heat transfer coefficients, and $A_{ref}$, $A_{air}$ are the heat transfer surface areas on the refrigerant and air sides, respectively. $R_{wall}$ accounts for thermal resistance through the exchanger wall. The convective coefficients are estimated from Nusselt number correlations based on local flow conditions. This approach is consistently applied to all heat exchangers in the refrigerant loop.

## 3.6 Cabin Thermal Modeling

Passenger thermal comfort in vehicle cabins depends on factors such as clothing, journey duration, cabin air temperature, and ambient climate. Among these, cabin air temperature is a critical and controllable parameter, as it directly governs heat exchange between occupants and their environment [32]. In this study, thermal comfort is assumed to be achieved when the cabin air temperature $T_{cair}$ tracks a reference setpoint. Cabin air temperature dynamics are influenced by three primary heat transfer mechanisms: heat exchange between passengers and cabin air ($\dot{Q}_{human}$), convective/conductive heat transfer from interior surfaces (glass, doors, roof), and HVAC airflow ($\dot{m}_{air}$) supplying conditioned air at temperature $T_{vent}$.
A two-node lumped parameter model is used to represent the thermal dynamics of the cabin, consisting of the cabin interior temperature $T_{int}$ and the cabin air temperature $T_{cair}$ [20, 33]. The thermal resistances $R_{glass}$, $R_{doors}$, and $R_{roof}$ are estimated based on geometry, material properties, and convective coefficients.

These resistances are computed as

$$R_{\mathrm{k}} = \alpha_k \left( \frac{1}{h_{\mathrm{k}} A_{\mathrm{k}}} + \frac{T_{\mathrm{k}}}{k_{\mathrm{k}} A_{\mathrm{k}}} \right), \quad k \in \{\mathrm{glass}, \mathrm{doors}, \mathrm{roof}\} \tag{28}$$

where $h_k$ is the convective heat transfer coefficient, $A_k$ is the surface area, $T_k$ is the material thickness, and $k_k$ is the thermal conductivity of the respective components. The total thermal resistance of the cabin envelope, $R_{\mathrm{total}}$, is calculated as the sum of individual resistances.
The cabin interior temperature dynamics is expressed as

$$M_{\mathrm{int}} c_{\mathrm{p,int}} \frac{\mathrm{d}T_{\mathrm{int}}(t)}{\mathrm{d}t} = \left( \alpha_1 \frac{T_{\mathrm{amb}}(t) - T_{\mathrm{int}}(t)}{R_{\mathrm{total}}} + \alpha_2 \frac{T_{\mathrm{air}}(t) - T_{\mathrm{int}}(t)}{R_{\mathrm{total}}} \right) \tag{29}$$

where, $c_{\mathrm{p,int}}$ is the specific heat capacity of the interior, estimated as a mass-weighted average of interior materials and $M_{\mathrm{int}}$ is the total mass of all the interior components.
The cabin air temperature dynamics and air mass flow rate are expressed as

$$C_{\mathrm{air}} \frac{\mathrm{d}T_{\mathrm{cair}}(t)}{\mathrm{d}t} = \alpha_3 \Big( \dot{m}_{\mathrm{air}}(t) c_{p,\mathrm{air}} (T_{\mathrm{vent}}(t) - T_{\mathrm{cair}}(t)) + \dot{Q}_{\mathrm{h}} + \alpha_4 \frac{T_{\mathrm{int}}(t) - T_{\mathrm{cair}}(t)}{R_{\mathrm{total}}} \Big), \;\; \dot{m}_{\mathrm{air}}(t) = \alpha_5 \dot{V}_{\mathrm{ref}} \rho_{\mathrm{air}} \frac{\omega_{\mathrm{bl}}(t)}{\omega_{\mathrm{bl,ref}}} \tag{30}$$

where $C_{\mathrm{air}} = V_{\mathrm{cab}} \rho_{\mathrm{air}} c_{p,\mathrm{air}}$ is the thermal capacitance of the cabin air, $T_{\mathrm{vent}}$ is the HVAC supply air temperature, and $\dot{V}_{\mathrm{ref}}$, $\omega_{\mathrm{bl,ref}}$ are reference values for volumetric flow rate and blower speed, respectively. The parameters $\alpha_1$ to $\alpha_5$ are tuning coefficients calibrated to match the cabin thermal behavior.

# 4 Model Parameter Identification

The goal of the COM is to capture the key dynamics of the high-fidelity reference model while remaining computationally efficient for real-time control. To achieve this, the model incorporates several simplifications and assumptions, as outlined in Section 3. To address these simplifications and ensure the model output remains representative of the reference system, a systematic parameter tuning process is employed. The tuning parameters are identified using an optimization-based approach that minimizes the weighted squared error between the predicted state trajectories of the COM and those of the high-fidelity MathWorks benchmark over the entire simulation horizon.
The nonlinear system dynamics of the MathWorks TEM model are described as

$$x_{\mathrm{M}}(t^+) = f_{\mathrm{M}}\left(x_{\mathrm{M}}(t), u_{\mathrm{M}}(t), d(t)\right) \tag{31}$$

where $x_{\mathrm{M}}$ is the state vector, $u_{\mathrm{M}}$ the control input vector, and $d$ the disturbance vector containing exogenous inputs such as vehicle speed and ambient temperature.
The COM dynamics are defined as

$$\dot{x}(t) = f\left(x(t), u(t), d(t), \Upsilon\right) \tag{32a}$$

where $d(t)$ represents the disturbance vector and $\Upsilon$ denotes the parameter vector. The simplified dynamics $f(\cdot)$ combine first-principles modeling with empirical component performance data. To achieve model accuracy, the parameter vector $\Upsilon$ must be calibrated such that the output of the COM matches closely with the corresponding outputs of the MathWorks reference model, denoted by $y_{\mathrm{M}}\left(x_{\mathrm{M}}(t), u_{\mathrm{M}}(t), d(t)\right)$.
The parameter identification problem is formulated as a nonlinear least-squares optimization

$$\min_{\Upsilon} \quad \int_0^T e(t,\Upsilon)^\top Q(t) e(t,\Upsilon)\, \mathrm{d}t \tag{33a}$$

$$\text{subject to} \quad x_{\mathrm{M}}(t^+) = f_{\mathrm{M}}\left(x_{\mathrm{M}}(t), u_{\mathrm{M}}(t), d(t)\right),\; x_{\mathrm{M}}(0) = x_{\mathrm{M},0} \tag{33b}$$

$$\dot{x}(t) = f\left(x(t), u(t), d(t), \Upsilon\right),\; x(0) = x_0 \tag{33c}$$

The modeling error $e(t,\Upsilon)$ is defined as

$$e(t,\Upsilon) = y_{\mathrm{M}}\left(x_{\mathrm{M}}(t), u_{\mathrm{M}}(t), d(t)\right) - \begin{bmatrix} x^\top(t) & u^\top(t) \end{bmatrix}^\top$$

where, $\Upsilon = \begin{bmatrix} \beta^\top & \vartheta^\top & \sigma^\top & \alpha^\top & \kappa^\top & \mu^\top & \psi^\top \end{bmatrix} \in$ represents the parameter vector, $Q$ is a time-varying positive definite weighting matrix and $x_{M,0}$ and $x_0$ are initial states of the reference and control models. The parameter vector $\Upsilon$ includes subvector contains model-specific parameters related to scaling factors, thermal resistances, battery electrical behavior, refrigerant-compressor characteristics, and heat transfer coefficients. The weighting matrix $Q$ enables emphasis on specific operational regimes: transient conditions for slow dynamics (e.g., state-of-charge) and steady-states for fast dynamics (e.g., cabin air temperature). Reference model states $x_M$ are obtained through offline simulation. Control model states $x$ depend implicitly on $\Upsilon$ through numerical integration. By selecting suitable choices for the disturbance and control inputs, the parameters' fitting in problem (33) can be solved either for simple cases, such as step inputs, or over standard driving cycles, such as the Worldwide Harmonized Light Vehicles Test Cycle (WLTC).

# 5 Model Validation

The proposed COM is validated against the high-fidelity MathWorks reference model using the extended WLTC driving cycle under cold ambient conditions ($-10\,^\circ$C). The primary goal is to accurately capture key thermal states–namely, battery, motor, and cabin air temperatures–such that the control model closely replicates the behavior of the high-fidelity reference. Although refrigerant pressure states are not the main focus, their accuracy is also assessed to ensure overall model integrity.

Component temperature trajectories demonstrate strong agreement between the two models. As illustrated in Fig. 2, the COM effectively captures the warm-up dynamics and steady-state values, maintaining a mean absolute error (MAE) below 1.45 °C across all major components.

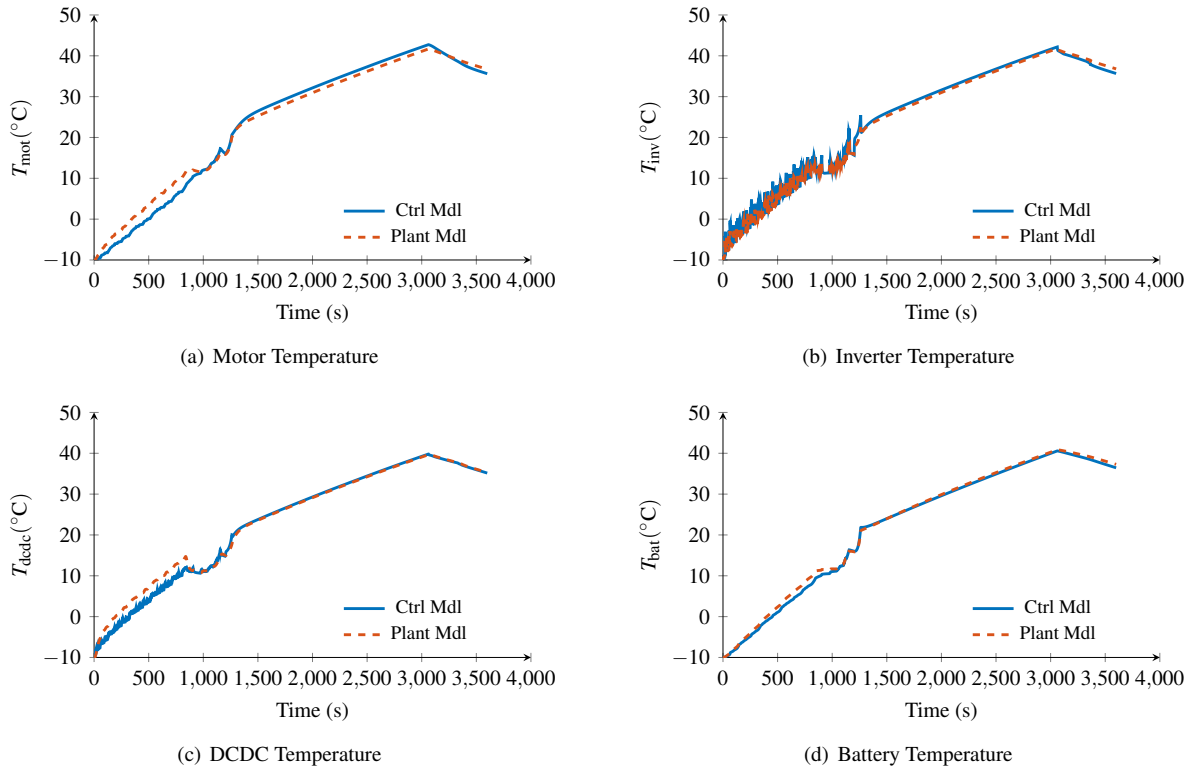


(a) Motor Temperature

(b) Inverter Temperature

(c) DCDC Temperature

(d) Battery Temperature

**Fig. 2.** Validation of component thermal states using the control-oriented model compared to the high-fidelity reference. The figure shows that the control model captures the thermal dynamics of the motor, inverter, DC-DC converter, and battery with high fidelity over the complete drive cycle.

Cabin air temperature results also exhibit high fidelity. As seen in Fig. 3, the control model tracks both transient and steady-state phases with an MAE of only 0.95 °C, supporting its suitability for use in passenger comfort control applications.

Validation metrics for all key states are summarized in Table 2. While the refrigerant pressure states exhibit slightly

higher deviations, this can be attributed to the simplified modeling of pressure dynamics–particularly the rate of change of pressure in the evaporator and condenser volumes. Nonetheless, the absolute errors remain within acceptable bounds for supervisory-level thermal control applications.

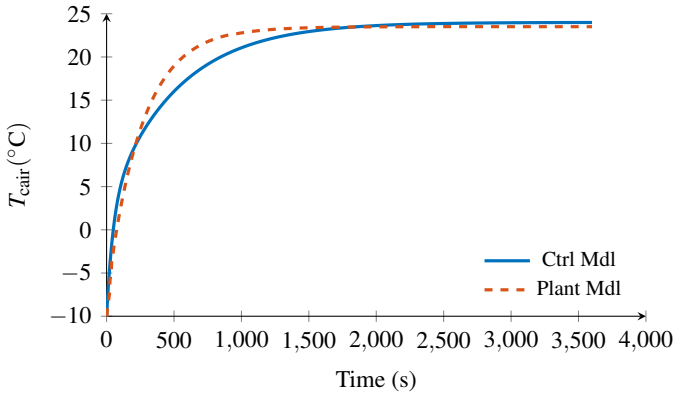


**Fig. 3.** Comparison of cabin air temperature profiles between the control-oriented and high-fidelity models under cold ambient conditions. The control model accurately tracks both transient warm-up and steady-state phase, achieving a MAE under 1 °C, which supports its use in cabin comfort control strategies.

**Table 2.** Validation metrics for control-oriented model against high-fidelity reference

| State | RMSE | MAE |
|---|---|---|
| Motor Temperature | 1.69 | 1.40 |
| Inverter Temperature | 0.93 | 0.73 |
| DCDC Temperature | 1.46 | 0.86 |
| Battery SOC | 0.00 | 0.00 |
| Battery Temperature | 0.71 | 0.55 |
| Compressor Inlet Pressure | 0.21 | 0.19 |
| Compressor Outlet Pressure | 3.79 | 2.85 |
| Cabin Interior Temperature | 3.20 | 3.03 |
| Cabin Air Temperature | 1.32 | 0.95 |

All simulations were performed in `MATLAB R2024b` on a Windows 11 64-bit system equipped with an Intel® Core™ i7-11850H CPU (8 cores, @ 2.5 GHz) and 32 GB RAM. Compared to the reference model, the proposed COM achieves an approximate 85% reduction in simulation time. This demonstrates its practical suitability for embedded deployment and predictive thermal management control applications.

# 6 Conclusion

This paper presents a control-oriented modeling framework for thermal energy management in battery electric vehicles (BEVs), focusing on architectures with reconfigurable coolant loops and heat pump-based HVAC systems. The proposed model, derived from a high-fidelity MathWorks reference, captures key thermal dynamics with high accuracy while significantly reducing computational complexity. Validation against the benchmark model demonstrates mean absolute errors below 1.5 °C for key thermal states and refrigerant pressures, alongside an 85% reduction in simulation time. These results confirm the models suitability for real-time implementation and advanced control applications.

The models modular structure and physical transparency make it well-suited for integration with predictive control strategies like MPC. Its open-source implementation further promotes transparency, reproducibility, and collaboration within the research community.

Future work will focus on extending the model to account for dynamic ambient conditions and deploying it within a real-time RTI-based MPC framework for predictive thermal energy management.

## Acknowledgments

The authors would like to thank their colleagues at Zeekr Technology Europe and Chalmers University of Technology for their valuable support and insightful input throughout the course of this research. Their contributions have been instrumental in shaping both the direction and outcomes of this study. This work was supported by funding from the Swedish Energy Agency (Energimyndigheten) and Zeekr Technology Europe.

## References

[1] European Union, "Regulation (eu) 2019/631 setting $co_2$ emission performance standards for new passenger cars and for new light commercial vehicles," 2019, official Journal of the European Union.

[2] M. Neaimeh, S. D. Salisbury, G. A. Hill, P. T. Blythe, D. R. Scoffield, and J. E. Francfort, "Analyzing the usage and evidencing the importance of fast chargers for the adoption of battery electric vehicles," *Energy Policy*, vol. 108, pp. 474–486, 2017.

[3] L. Noel and B. K. Sovacool, "Examining the social acceptance of electric mobility: A review of the literature on driver preferences, purchase intentions, and willingness to pay," *Transp. Res. D: Transp. Environ.*, vol. 72, pp. 255–274, 2019.

[4] D. Pevec, J. Babic, A. Carvalho, Y. Ghiassi-Farrokhfal, W. Ketter, and V. Podobnik, "A survey-based assessment of how existing and potential electric vehicle owners perceive range anxiety," *Journal of Cleaner Production*, vol. 276, p. 122779, 2020.

[5] E. Paffumi, M. De Gennaro, G. Martini, and U. Manfredi, "Experimental test campaign on a battery electric vehicle: On-road test results (part 2)," *SAE Int. J. Alt. Power*, vol. 4, no. 2, pp. 277–292, 2015.

[6] M. A. Jeffers, L. Chaney, and J. P. Rugh, "Climate control load reduction strategies for electric drive vehicles in warm weather," *SAE Technical Paper Series*, no. 2016-01-0262, 2016.

[7] B. Zhang, T. Zhang, L. Gao, and C. Zhu, "Performance analysis and optimization of an air source heat pump system for electric vehicle cabin heating," *Energy Convers. Manage.*, vol. 172, pp. 492–502, 2018.

[8] Y. Xie, W. Chen, and R. Cao, "Experimental investigation on a heat pump system with additional auxiliary water-heating cycle for electric vehicles," *Appl. Therm. Eng.*, vol. 164, p. 114513, 2020.

[9] J. J. Meyer, J. Lustbader, N. Agathocleous, A. Vespa, J. Rugh, and G. Titov, "Range extension opportunities while heating a battery electric vehicle," *SAE Technical Paper Series*, no. 2018-01-0066, 2018.

[10] S. Schaut and O. Sawodny, "Thermal management for the cabin of a battery electric vehicle considering passengers comfort," *IEEE Transactions on Control Systems Technology*, vol. 28, no. 4, pp. 1476–1492, 2019.

[11] D. Kibalama, Y. Liu, S. Stockar, and M. Canova, "Model predictive control for automotive climate control systems via value function approximation," *IEEE Control Systems Letters*, vol. 6, pp. 1820–1825, 2022.

[12] Y. Xie, Z. Liu, K. Li, J. Liu, Y. Zhang, D. Dan, C. Wu, P. Wang, and X. Wang, "An improved intelligent model predictive controller for cooling system of electric vehicle," *Applied Thermal Engineering*, vol. 182, p. 116084, 2021. [Online]. Available: https://doi.org/10.1016/j.applthermaleng.2020.116084

[13] M. Alizadeh, S. Dhale, and A. Emadi, "Model predictive control of HVAC system in a battery electric vehicle with fan power adaptation for improved efficiency and online estimation of ambient temperature," in *IECON 2021 47th Annual Conference of the IEEE Industrial Electronics Society*, 2021, pp. 1–6.

[14] F. Ju, N. Murgovski, W. Zhuang, and L. Wang, "Integrated propulsion and cabin-cooling management for electric vehicles," *Actuators*, vol. 11, no. 12, 2022. [Online]. Available: https://www.mdpi.com/2076-0825/11/12/356

[15] M. A. Jeffers, L. Chaney, and J. P. Rugh, "Climate control load reduction strategies for electric drive vehicles in cold weather," *SAE International Journal of Passenger Cars-Mechanical Systems*, vol. 9, no. 2016-01-0262, pp. 75–82, 2016.

[16] S. Park and C. Ahn, "Computationally efficient stochastic model predictive controller for battery thermal management of electric vehicle," *IEEE Transactions on Vehicular Technology*, vol. 69, no. 8, pp. 8407–8419, Aug. 2020.

[17] J. Lopez-Sanz, C. Ocampo-Martinez, J. Alvarez-Florez, M. Moreno-Eguilaz, R. Ruiz-Mansilla, J. Kalmus, M. Gräeber, and G. Lux, "Nonlinear model predictive control for thermal management in plug-in hybrid electric vehicles," *IEEE Transactions on Vehicular Technology*, vol. 66, no. 5, pp. 3632–3644, 2017.

[18] S. Bauer, A. Suchaneck, and F. Puente León, "Thermal and energy battery management optimization in electric vehicles using pontryagin's maximum principle," *Journal of Power Sources*, vol. 246, pp. 808–818, 2014. [Online]. Available: https://www.sciencedirect.com/science/article/pii/S0378775313013591

[19] Y. Wu, Z. Huang, D. Li, H. Li, J. Peng, D. Stroe, and Z. Song, "Optimal battery thermal management for electric vehicles with battery degradation minimization," *Applied Energy*, vol. 353, p. 122090, 2024. [Online]. Available: https://www.sciencedirect.com/science/article/pii/S030626192301454X

[20] P. Lokur, N. Murgovski, and M. Larsson, "Control-oriented model for thermal energy management of battery electric vehicles," *IEEE Transactions on Vehicular Technology*, 2024.

[21] MathWorks, "Electric vehicle thermal management with heat pump," 2024, accessed: 07/11/2024. [Online]. Available: https://www.mathworks.com/help/autoblks/ug/electric-vehicle-thermal-management-with-heat-pump.html

[22] A. Sciarretta and L. Guzzella, "Control of hybrid electric vehicles," *IEEE Control Syst. Mag.*, vol. 27, no. 2, pp. 60–70, 2007.

[23] A. Afram and F. Janabi-Sharifi, "Theory and applications of hvac control systems a review of model predictive control (mpc)," *Building and Environment*, vol. 72, pp. 343–355, 2014.

[24] L. Guzzella, A. Sciarretta *et al.*, *Vehicle propulsion systems*. Springer, 2007, vol. 1.

[25] M. H. Bierhoff and F. W. Fuchs, "Semiconductor losses in voltage source and current source igbt converters based on analytical derivation," in *2004 IEEE 35th Annual Power Electronics Specialists Conference (IEEE Cat. No. 04CH37551)*, vol. 4. IEEE, 2004, pp. 2836–2842.

[26] Y. Xu, *Novel Powertrain Topologies for Energy-Efficient Battery Electric Vehicles*. Chalmers Tekniska Hogskola (Sweden), 2023.

[27] Y. Zhu, M. Xiao, X. Su, G. Yang, K. Lu, and Z. Wu, "Modeling of conduction and switching losses for igbt and fwd based on svpwm in automobile electric drives," *Applied Sciences*, vol. 10, no. 13, p. 4539, 2020.

[28] G. L. Davis, F. Chianese, and T. C. Scott, "Computer simulation of automotive air conditioningcomponents, system, and vehicle," SAE International, SAE Technical Paper 720043, 1972.

[29] T. Scott and S. Sundaram, "Robust compressor model for ac system simulation," *SAE Transactions*, pp. 458–463, 2007.

[30] Q. Zhang, S. Stockar, and M. Canova, "Energy-optimal control of an automotive air conditioning system for ancillary load reduction," *IEEE Transactions on Control Systems Technology*, vol. 24, no. 1, pp. 67–80, 2015.

[31] Y. A. Cengel, "Heat transfer a practical approach," 2003.

[32] X. Zhou, D. Lai, and Q. Chen, "Experimental investigation of thermal comfort in a passenger car under driving conditions," *Building and Environment*, vol. 149, pp. 109–119, 2019. [Online]. Available: https://doi.org/10.1016/j.buildenv.2018.12.022

[33] P. Lokur, K. Nicklasson, L. Verde, M. Larsson, and N. Murgovski, "Modeling of the thermal energy management system for battery electric vehicles," in *2022 IEEE Vehicle Power and Propulsion Conference (VPPC)*. IEEE, 2022, pp. 1–7.

# Presenter Biography

**Prashant Lokur** is an Industrial PhD student jointly affiliated with the Department of Energy and Thermal Management at Zeekr Technology Europe and the Division of Systems and Control, Department of Electrical Engineering, Chalmers University of Technology, Sweden. He received his bachelor's degree in Mechanical Engineering from VTU, India, in 2012, and his master's degree in Systems, Control, and Mechatronics from Chalmers University of Technology in 2015. His current research focuses on the development of optimal control strategies for thermal energy management in battery electric vehicles.

**Nikolce Murgovski** is a Professor with the Division of Systems and Control, Department of Electrical Engineering, Chalmers University of Technology. He received an M.S. degree in Software Engineering from University West, Trollhättan, in 2007, and both an M.S. degree in Applied Physics and a PhD degree in Systems and Control from Chalmers University of Technology in 2007 and 2012, respectively. His research interests include optimization, optimal control, modeling, online learning, and estimation, with applications in electromobility, autonomous driving, and active safety systems in automotive engineering.

**Mikael Larsson** is currently a Senior Developer Consultant in the automotive industry. At the time of this work, he was with the Department of Energy and Thermal Management at Zeekr Technology Europe, where he was an integral part of the thermal management software development team since its inception in 2020. He received his bachelor's degree in Automation and Mechatronics and his master's degree in Communication Engineering from Chalmers University of Technology, Gothenburg, Sweden, in 2013 and 2015, respectively.